Synthesis, Characterization, and Reactivity toward Dioxygen of Copper Manganese Cofacial Porphyrins. Crystal and Molecular Structures of a Heterobimetallic Biphenylene-Pillared Cofacial Diporphyrin

Roger Guilard,*[1a] Stéphane Brandes,[1a] Alain Tabard,[1a] Nouhza Bouhmaida,[1b] Claude Lecomte,[1b] Philippe Richard,[1a] and Jean-Marc Latour[1c]

Contribution from the Laboratoire d'Ingénierie Moléculaire pour la Séparation et les Applications des Gaz, "LIMSAG" (UMR 9953), Faculté des Sciences "Gabriel", Université de Bourgogne, 6 boulevard Gabriel, 21100 Dijon, France, Laboratoire de Minéralogie et Cristallographie, "LMCPI" (URA CNRS 809), Université Henri Poincaré I, B.P. 239, 54506 Vandoeuvre les Nancy, France, and Département de Recherche Fondamentale sur la Matière Condensée et Service d'Etude des Systèmes et Architectures Moléculaires, Laboratoire de Chemie de Coordination (URA 1194), Centre d'Etudes Nucléaires de Grenoble, 85X-F 38041 Grenoble Cedex, France

*Received September 14, 1993**

Abstract: The synthesis of a novel family of heterobinuclear cofacial biphenylene-bridged or anthracene-bridged bisporphyrin, (DP)CuMnX, is reported, DP being either 1,8-bis(2,8,13,17-tetraethyl-3,7,12,18-tetramethylporphyrin-5-yl)biphenylene, DPB, or 1,8-bis(2,8,13,17-tetraethyl-3,7,12,18-tetramethylporphyrin-5-yl)anthracene, DPA. Each complex has been characterized by mass spectrometry, UV-vis, IR, and ESR spectroscopies, and magnetic measurements. Metal-metal interactions are clearly established on the basis of various spectroscopic data. At room temperature the copper(II)-manganese(II) diporphyrin biphenylene complex forms a reversible dioxygen adduct. Moreover, the molecular structure of (DPB)CuMnCl has been solved by X-ray diffraction. (DPB)CuMnCl·C_8H_{10} ($C_{76}H_{76}N_8CuMnCl·C_8H_{10}$) crystallizes in the triclinic system, space group $P\bar{1}$ with lattice constants a = 13.232(5) Å, b = 15.228(6) Å, c = 18.997(5) Å, α = 103.22(3)°, β = 101.63(3)°, γ = 94.86(3)°, V = 3615 Å^3, Z = 2, $R(F)$ = 6.95%, $R_w(F)$ = 6.75%, and GOF = 1.47 for 2942 reflections with $I \geq 3\sigma(I)$. In (DPB)CuMnCl, the metal-metal distance is 4.127(3) Å and both porphyrin moieties are slipped by α = 25.8°.

Much attention is being devoted to the discovery of new efficient catalysts for multielectron reduction of O_2 or N_2. The preparation of binuclear metallic porphyrin complexes exhibiting metal-metal interaction is of major interest for molecular oxygen activation. Such compounds represent a class of very well studied bioinorganic models for many essential biological systems,[2-6] such as cytochrome *c* oxidase and monooxygenase enzymes.[7-10] Moreover, metalloporphyrins exhibiting metal-metal bonds or metal-metal interactions have been the subject of intense research, but most of the complexes with metal-metal bonds are quite unstable.[11,12] In order to enhance the stability of the bimetallic edifice, we have used bimetalloporphyrin entities where the macrocycles are bridged by a rigid spacer. Previous studies showed that the cofacial porphyrins (DPA)H_4 and (DPB)H_4 [DPA = 1,8-bis(2,8,13,17-tetraethyl-3,7,12,18-tetramethylporphyrin-5-yl)anthracene and DPB = 1,8-bis(2,8,13,17-tetraethyl-3,7,12,18-tetramethylporphyrin-5-yl)biphenylene] satisfied the above requirement. These bisporphyrinic ligands are commonly named "Pacman" porphyrin due to the structural analogy with the "glutton" of a video game.

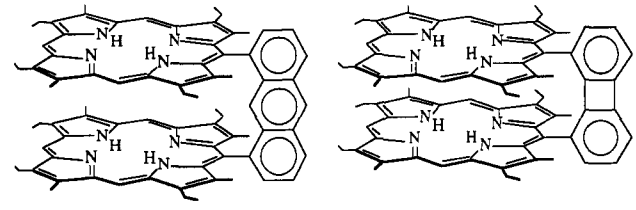

(DPA)H_4 (DPB)H_4

Our work is focused on heterobimetallic compounds in which a copper(II) ion is juxtaposed to a manganese ion. In fact these two elements are likely to favor a donor and acceptor interaction via the cavity and then should be a quite good model of cytochrome *c* oxidase. It is also well known that low oxidation states are of primary importance mainly in the function of biological systems, like the reversible fixation of dioxygen. Up to now extensive studies have been carried out on synthetic oxygen carriers based on Co^{II} and Fe^{II},[13] but less work has been reported concerning the use of Mn^{II} complexes as oxygen carriers.[2,14] It is well established that most of the iron(II) and manganese(II) porphyrins reversibly bind dioxygen only at low temperature (-78 °C) while these complexes are irreversibly oxidized to μ-oxo complexes at room temperature. In order to stabilize the oxygenated species (Por)Mn(O_2), copper(II) manganese(II) bisporphyrins are of

* Abstract published in *Advance ACS Abstracts,* October 1, 1994.

(1) (a) Université de Bourgogne. (b) Université de Nancy. (c) Centre d'Etudes Nucléaires de Grenoble.

(2) Jones, D. R.; Summerville, D. A.; Basolo, F. *Chem. Rev.* **1979**, *79*, 139-179.
(3) Malmstrõm, G. *Chem. Rev.* **1990**, *90*, 1247-1260.
(4) Ibers, J. A.; Holm, R. H. *Science* **1980**, *209*, 223-235.
(5) Buchler, J. W. *Angew. Chem., Int. Ed. Engl.* **1978**, *17*, 407-423.
(6) Peisach, J.; Blumberg, W. E.; Adler, A. *Ann. N.Y. Acad. Sci.* **1973**, *206*, 310-327.
(7) Bulach, V.; Mandon, D.; Weiss, R. *Angew. Chem., Int. Ed. Engl.* **1991**, *30*, 572-575.
(8) Koch, C. A.; Reed, C. A.; Brewer, G. A.; Rath, N. P.; Scheidt, W. R.; Gupta, G.; Lang, G. *J. Am. Chem. Soc.* **1989**, *111*, 7645-7648.
(9) Sakurai, H.; Yoshimura, T. *J. Inorg. Biochem.* **1985**, *24*, 75-96.
(10) Battersby, A. R.; Hamilton, A. D. *J. Chem. Soc., Chem. Commun.* **1980**, *117*-119.
(11) Guilard, R.; Lecomte, C.; Kadish, K. M. *Struct. Bonding* **1987**, *64*, 205-268.
(12) Guilard, R.; Kadish, K. M. *Comments Inorg. Chem.* **1988**, *7*, 287-305.
(13) Basolo, F.; Hoffman, B. M.; Ibers, J. A. *Acc. Chem. Res.* **1975**, *8*, 384-392.
(14) Naruta, Y.; Maruyama, K. *J. Am. Chem. Soc.* **1991**, *113*, 3595-3596.

0002-7863/94/1516-10202$04.50/0

primary interest. Indeed the electron-rich bisporphyrin cavity and the proximity of the copper(II) ion to manganese(II) could favor the formation of the oxygenated species at room temperature. In this paper, we describe the synthesis and characterization of a novel heterodinuclear family, (DP)CuMnCl and (DP)CuMnL, where DP^{4-} is the tetraanion of the biphenylenyldiporphyrin DPB, or the anthracenyldiporphyrin DPA, and L an axial ligand coordinated to the manganese atom (L = 1-*tert*-butyl-5-phenylimidazole). Each complex has been characterized by mass spectrometry, UV–vis, IR, and ESR spectroscopies, and magnetic measurements, and the molecular structure of (DPB)CuMnCl was solved by X-ray diffraction.

Experimental Section

Chemicals. All reagents and solvents used were of commercial grade. Toluene was distilled under argon on the sodium benzophenone complex. Methanol used for manganese(II) complexes was distilled on $CaCl_2$ under argon and then dried over 3 Å molecular sieves. 1-*tert*-Butyl-5-phenylimidazole (labeled L throughout the paper) was prepared by the Van Leusen method[15] and purified by sublimation.

Instrumentation. UV–vis spectra were recorded on a Varian Cary 1 spectrometer. Infrared spectra were obtained on a Perkin-Elmer 580B apparatus. Solid samples were prepared as a 1% dispersion in CsI. ESR spectra were recorded on a Bruker ESP300 spectrometer (Centre de Spectrométrie Moléculaire de l'Université de Bourgogne) or on a Varian E-4 spectrometer equipped with an Oxford Instruments cryostat, operating at 9.2 gHz with a power of 0.1–1 mW and a modulation of 10 G (Centre d'Etudes Nucléaires de Grenoble). The calibration was done using diphenylpicrylhydrazyl (DPPH) as the standard. Mass spectra were obtained with a Kratos Concept 32 S spectrometer in the DCIMS mode (gas: ammonia or isobutane). The data were collected and processed using a Sun 3/80 workstation. The magnetic susceptibility experiments have been performed on a Quantum Design MPMS magnetometer from 2 to 300 K at a field of 0.5 T. The samples (15–20 mg) were contained in a Kel F bucket. The bucket had been calibrated independently at the same field and temperatures. The data of (DPA)CuMnCl were fitted to the following equation (see the Results and Discussion for explanation): $\chi T = g^2\beta^2/4k\{\exp(-8D/3kT) + 9\exp(-2D/3kT) + 25\exp(10D/3kT) + \exp[(J-D')/3kT] + 9\exp[(J+D')/3kT]\}/\{\exp(-8D/3kT) + \exp(-2D/3kT) + \exp(10D/3kT) + \exp[(J-D')/3kT] + \exp[(J+D')/3kT]\}$. The quantity minimized was

$$R = \frac{\sum[(\chi_{exp}T)^2 - (\chi_{calc}T)]^2}{N\sum[(\chi_{exp}T)^2]}$$

The R index amounted to 1.37×10^{-5}.

Syntheses of (DPA)H_4 (1) and (DPB)H_4 (2). The ligands have been prepared according to the modified methods previously described.[16-18]

Syntheses of (DPA)ZnH_2 (3) and (DPB)ZnH_2 (4). The synthesis of these compounds was done as previously reported.[17,18]

Synthesis of (DPA)CuH_2 (5). To (DPA)ZnH_2 (250 mg, 0.21 mmol) in CH_2Cl_2 (200 cm^3) under stirring is added a methanol solution of copper acetate monohydrate (50 cm^3, 1 g·L^{-1}), and the reaction is completed after 30 min. The solvent is evaporated and the compound crystallized as methanol solvent is added. After filtration and washing with methanol, the purple crystals are dissolved in CH_2Cl_2 (50 cm^3). A solution of HCl (5 cm^3, 6 M) is added under vigorous stirring for 15 min, and the solution is neutralized with a 10% solution of sodium carbonate. The organic layer is washed three times with water, dried over $MgSO_4$, and then partially evaporated. Addition of methanol to the concentrated solution gives a purple crystalline powder. Yield: 96%. DCIMS: m/z = 1193 ([M + H]$^+$). IR: 3278 cm^{-1} (NH).

Table 1. X-ray Data for (DPB)CuMnCl·C_8H_{10}

formula	$C_{76}H_{76}N_8CuMnCl\cdot C_8H_{10}$
formula weight, g·mol^{-1}	1360.92
space group	triclinic $P\bar{1}$
cell dimensions	
a, b, c, Å	13.232(5), 15.228(6), 18.997(5)
α, β, γ, deg	103.22(3), 101.63(3), 94.86(3)
V (Å^3), Z, F_{000} (e$^-$)	3615, 2, 1434
d_{calcd} (g·cm^{-3}), μ (cm^{-1})	1.250, 5.152
crystal dimensions, mm^3	0.2 × 0.15 × 0.1
radiation	Mo Kα, λ = 0.7107 Å
scan type	ω
scan width, deg	2.6 + 0.35 tan θ
aperture $V \times H$, mm	6 × 5
scan speed, deg·mn^{-1}	constant speed 1.37
$(\sin\theta)/\lambda_{max}$, Å^{-1}	0.57
hkl	
lower limit	−15,−17,0
upper limit	15,17,21
std reflcns	222, 429, 151, 231
no. of reflcns measd	10 587
no. of unique reflcns ($I \geq 3\sigma(I)$)	2942
$I \geq 2\sigma(I)$	3901

Synthesis of (DPB)CuH_2 (6). To a refluxing solution of (DPB)H_4 (500 mg, 0.45 mmol) in CH_2Cl_2 (230 cm^3) is added dropwise a solution of copper(II) acetate monohydrate (50 cm^3, 2 g·L^{-1}) in methanol. The reaction is monitored by TLC (silica, CH_2Cl_2/MeOH (9:1) as eluent). Addition is stopped when no free base can be detected on TLC. The solution is then evaporated and the residue chromatographed on silica gel with 2–10% MeOH/CH_2Cl_2 eluent. Addition of methanol followed by evaporation of dichloromethane gives a purple crystalline powder. Yield: 67%. DCIMS: m/z = 1167 ([M + H]$^+$). IR: 3281 cm^{-1} (NH).

Synthesis of (DPA)CuMnCl (7). The metalation follows Adler's method.[19] Compound **5** (460 mg, 0.39 mmol) is dissolved in refluxing DMF (230 cm^3), and manganese(II) chloride tetrahydrate is then added (390 mg, 1.95 mmol). After 10 h, the UV–vis spectrum of the mixture shows the absorption band at 478 nm characteristic of the manganese(III) porphyrin complex. The completion of the reaction is achieved by the addition of an extra amount of $MnCl_2$ (390 mg), and then the solution is refluxed for 5 h. The solution is evaporated, and the residue is dissolved in CH_2Cl_2 (200 cm^3) and washed five times with water. The organic layer is dried over $MgSO_4$ and the solvent evaporated. The crude material is chromatographed on a silica gel column with CH_2Cl_2/MeOH mixtures as eluents (20:1 to 10:1). The pure product is obtained with an 82% yield. DCIMS: m/z = 1281 ([M + H]$^+$). IR: 274 cm^{-1} (MnCl).

Synthesis of (DPB)CuMnCl (8). The same procedure as described for the DPA series is used. Yield: 88%. DCIMS: m/z = 12.25 ([M + H]$^+$). IR: 270 cm^{-1} (MnCl).

Synthesis of (DPA)CuMnL (9). The Mn^{III} complex is reduced to the Mn^{II} complex according to Reed's method.[20,21] A mixture of **7** (300 mg, 0.23 mmol), zinc amalgam (1 g) and 1-*tert*-butyl-5-phenylimidazole (230 mg, 1.16 mmol) is dissolved in degassed toluene (60 cm^3) and maintained under an argon atmosphere. The reaction mixture is heated to 100 °C under vigorous stirring. The absorption band of the Mn^{III} complex (480 nm) disappears after 2 h. The solution is filtered off on degassed Celite, and the solvent is removed under reduced pressure. The solid is then washed with MeOH and filtered. After drying under vacuum, 157 mg of pure product is obtained (0.137 mmol, 59%). DCIMS: 1245 ([M − L]$^+$).

Synthesis of (DPB)CuMnL (10). The above procedure is used for the preparation of compound **10**, and a similar yield is obtained. DCIMS: 1218 ([M − L]$^+$).

Crystal and Molecular Structures of (DPB)CuMnCl·C_8H_{10}. (DPB)-CuMnCl·C_8H_{10} crystallizes as small and very low quality triclinic single crystals as revealed by Weissenberg photographs. Cell parameters and intensity data were collected on an Enraf Nonius CAD4F diffractometer with graphite-monochromatized Mo Kα radiations; due to the crystal quality, ω scans as large as 2.6° were deemed necessary to collect the intensity data set (see Table 1 for more experimental details). The 10 584

(15) Van Leusen, A. M.; Schaart, F. J.; Van Leusen, D. *Recl.: J. R. Neth. Chem. Soc.* **1979**, *98*, 258–262.
(16) Chang, C. K.; Abdalmuhdi, I. *J. Org. Chem.* **1983**, *48*, 5388–5390.
(17) Collman, J. P.; Hutchison, J. E.; Lopez, M. A.; Tabard, A.; Guilard, R.; Seok, W. K.; Ibers, J. A.; L'Her, M. *J. Am. Chem. Soc.* **1992**, *114*, 9869–9877.
(18) Guilard, R.; Lopez, M. A.; Tabard, A.; Richard, P.; Lecomte, C.; Brandès, S.; Hutchison, J. E.; Collman, J. P. *J. Am. Chem. Soc.* **1992**, *114*, 9877–9889.
(19) Adler, A. D.; Longo, F. R.; Kampas, F.; Kim, J. *J. Inorg. Chem.* **1970**, *32*, 2443–2445.
(20) Landrum, J. T.; Hatano, K.; Scheidt, W. R.; Reed, C. A. *J. Am. Chem. Soc.* **1980**, *102*, 6729–6735.
(21) Reed, C. A.; Kouba, J. K.; Grimes, C. J.; Cheung, S. K. *Inorg. Chem.* **1978**, *17*, 2666–2670.

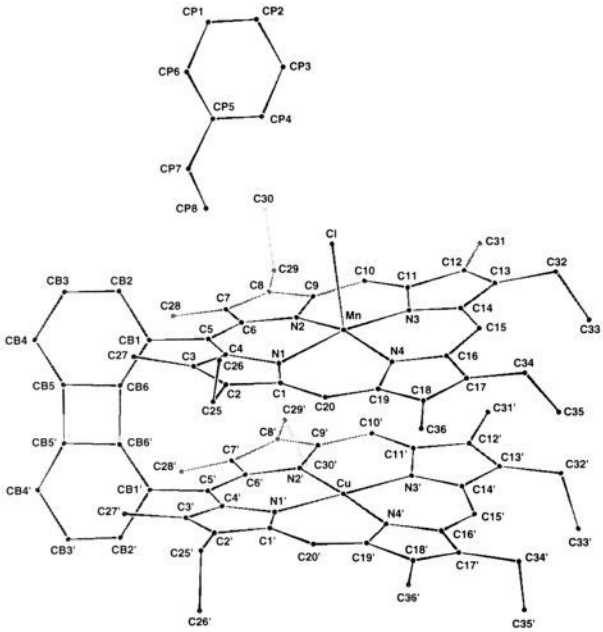

Figure 1. View and atom labeling of (DPB)CuMnCl·C_8H_{10}.

measured data were reduced with the SDP[22] programs; an almost linear loss of 22% of the four standard reflections was observed during the 441 h exposure time and intensity were corrected for. The structure was solved in the centrosymmetric $P\bar{1}$ space group by using conventional Patterson methods and subsequent Fourier and difference Fourier syntheses: a solvent ethylbenzene molecule (C_8H_{10}) was then located. The six carbon atoms of its phenyl ring were constrained[23] to a regular hexagon (C–C = 1.395 Å); hydrogen atoms were also included as fixed contributors in the least-squares process at their calculated positions. At the end of the refinement a Fourier difference map revealed that the C35′ atom of one ethyl group (see Figure 1) was disordered. This disorder was modeled by allowing two positions of this atom (C35′ and C35″) the occupancies of which were refined to 0.6 and 0.4. Due to the lack of data, the refinement[23] was made against the 3901 structure factors with $I \geq 2\sigma(I)$. At the end of the refinement the statistical indices of fit were $R(F) = 9.65\%$, $R_w(F) = 8.95\%$, and GOF = 1.53. These numbers decrease to 6.95%, 6.75%, and 1.47, respectively, when calculated (not refined) from the 2942 reflections with $I \geq 3\sigma(I)$. Table 2 gives the fractional coordinates and equivalent isotropic thermal motion parameters of the non-hydrogen atoms; Table 3 gives selected bond distances and angles in the molecule. Tables of anisotropic thermal motion parameters, full bond distances and angles, least-squares planes, and positional parameters for hydrogen atoms and a list of structure factors have been deposited as supplementary material.

Results and Discussion

Synthesis of (DP)CuMnCl and (DP)CuMnL Complexes Where DP = DPA or DPB and L = 1-*tert*-Butyl-5-phenylimidazole. The monocopper porphyrins **5** and **6** are synthesized by treating the free bases **1** and **2**, respectively, with 1 equiv of copper salt.[24] It is interesting to note that the dicopper derivatives are obtained in significant yield, mainly in DPA series for which the two porphyrins tend to behave as two independent macrocycles. Consequently, direct metalation of $(DPA)H_4$ leads to only a 40% yield of monometallic compound. This observation leads us to follow an alternative method by using zinc as the protective agent in one porphyrin ring.[25] Thus, $(DPA)ZnH_2$ is obtained in a 77% yield, and after treatment with copper(II) salt, the zinc–copper derivative is obtained in a quantitative yield. The action of a solution of 6 M HCl gives the monocopper derivative $(DPA)CuH_2$ (yield 74% on the basis of $(DPA)H_4$). Heteronuclear complexes (DP)CuMnCl are obtained by metalation of $(DP)CuH_2$ with $MnCl_2$. These reactions are summarized in Scheme 1.

Low oxidation state heterobimacrocycles $(DP)Cu^{II}Mn^{II}L$ are prepared by reduction of $(DP)Cu^{II}Mn^{III}Cl$ with zinc amalgam in toluene under an argon atmosphere in the presence of a bulky ligand which prevents any coordination inside the cavity. On the basis of previous work,[26] we have chosen 1-*tert*-butyl-5-phenylimidazole as the bulky ligand. The $(DP)Cu^{II}Mn^{II}L$ complexes are isolated in a 60% yield.

Crystal Structure of (DPB)CuMnCl. The molecular structure of (DPB)CuMnCl has been solved by X-ray methods. Figure 1 is a projection of the crystal structure of (DPB)CuMnCl·C_8H_{10} with the numbering scheme used. The conformation of this heterobimetallic Pacman porphyrin is very similar to those of (DPB)CoAl(OEt)[18] and $(DPB)Cu_2$.[27] As previously observed for these latter molecules the porphyrin moieties are slipped with respect to each other, leading to nonbonding metal–metal distances. In (DPB)CuMnCl, the Cu–Mn distance is 4.127(3) Å compared to 4.370(1) Å for Co–Al in (DPB)CoAl(OEt);[18] hence, no metal–metal bond occurs. The slip angle, α, the slip parameter, Sp, and the interring separation, Sr, as already defined[18] are, respectively, 25.8°, 1.71 Å, and 3.54 Å compared to 29.8°, 2.03, and 3.54 Å for (DPB)CoAl(OEt). It then appears that the angle between the normals of the two porphyrin rings is 5.2(1)°. The difference in the metal–metal distances observed between (DPB)CoAl(OEt) and (DPB)CuMnCl results from two effects: the different values of the α and Sp parameters while the interring separation Sr remains constant and the relative out of plane positions for the aluminum atom in (DPB)CoAlOEt (Δ4N = 0.365 Å) and manganese atom in (DPB)CuMnCl (Δ4N = 0.25 Å). The Mn–N ($\langle$Mn–N$\rangle$ = 2.01 ± 0.02 Å), Mn–Cl (2.382(5) Å), and Δ4N (0.25 Å) distances observed in this Pacman porphyrin are in excellent agreement with those of (TPP)MnCl.[28] A similar agreement is found for the Cu–N bond distances: in this study the mean value is 2.00 ± 0.03 Å compared to 1.981 Å in (TPP)Cu in which the porphinato core is very ruffled.[29] In this Pacman porphyrin the porphinato core is not planar, the maximum deviation from the mean plane being 0.42 Å. Finally the stereochemical parameters for the biphenylene connector agree with those found for other Pacman porphyrins.

The triclinic $P\bar{1}$ unit cell contains two diporphyrin molecules and two ethylbenzene solvates which are related by the inversion center as shown in Figure 2; the orientation of the solvate molecule is similar to that observed in (DPB)CoAl(OEt): the solvent molecules are almost perpendicular to the porphyrin plane and the closest contact is 3.65 Å between the ethylbenzene molecule and a methyl carbon atom of the manganese porphyrin (C35–CP3).

UV–Vis Spectroscopy. UV–vis characteristics of Pacman monometallic and heterobimetallic porphyrins are given in Tables 4 and 5 and Figure 3 represents the UV–vis spectra of $(DPB)H_4$, $(DPB)CuH_2$, and (DPB)CuMnCl recorded in CH_2Cl_2. The spectra of $(DP)CuH_2$ and (DP)CuMnCl are typical of monometallic and bimetallic complexes. The UV–vis spectrum of the free bases is of a "phyllo" type[30] with four bands. Compared to a similar nonsymmetrical monoporphyrin such as 5-phenyl-2,8,13,17-tetraethyl-3,7,12,18-tetramethylporphine $[(MPP)H_2]$,[16] $(DPB)H_4$ and $(DPA)H_4$ show a hypsochromic shift of the Soret band whereas each Q band is bathochromically shifted. Fur-

(22) *SDP*: *Structure Determination Package*; Enraf-Nonius: Delft, The Netherlands, 1977.
(23) Sheldrick, G. M. *SHELX 76*: *Program for Crystal Structure Determinations*; University of Göttingen: Göttingen, Federal Republic of Germany, 1976.
(24) Ni, C.-L.; Abdalmuhdi, I.; Chang, C. K.; Anson, F. C. *J. Phys. Chem.* **1987**, *91*, 1158–1166.
(25) Collman, J. P.; Garner, J. M. *J. Am. Chem. Soc.* **1990**, *112*, 166–173.
(26) Collman, J. P.; Hutchinson, J. E.; Lopez, M. A.; Guilard, R.; Reed, R. A. *J. Am. Chem. Soc.* **1991**, *113*, 2794–2796.
(27) Fillers, J. P.; Ravichandran, K. G.; Abdalmuhdi, I.; Tulinski, A.; Chang, C. K. *J. Am. Chem. Soc.* **1986**, *108*, 417–424.
(28) Tulinsky, A.; Chen, B. M. L. *J. Am. Chem. Soc.* **1977**, *99*, 3647–3651.
(29) Fleischer, E. B. *J. Am. Chem. Soc.* **1963**, *85*, 1353–1354.
(30) Smith, K. M. In *Porphyrins and Metalloporphyrins*; Smith, K. M., Ed.; Elsevier Scientific: Amsterdam, 1975; pp 3–28.

Table 2. Position Parameters and Estimated Standard Deviations for (DPB)CuMnCl·C_8H_{10}

atom	x	y	z	B (Å²)	atom	x	y	z	B (Å²)
Mn	0.0520(2)	0.2416(1)	0.6443(1)	3.62(6)	Cu	0.0065(1)	0.2287(1)	0.85048(9)	4.80(6)
Cl	0.1551(3)	0.2306(1)	0.5540(2)	5.0(1)	N1′	0.1383(9)	0.297(1)	0.9591(7)	5.0(4)
N1	0.1722(8)	0.3043(8)	0.7311(5)	3.7(3)	N2′	−0.0281(9)	0.3453(7)	0.8312(6)	3.9(3)
N2	0.0108(9)	0.3657(8)	0.6439(6)	3.6(3)	N3′	−0.128(1)	0.162(1)	0.7797(7)	5.3(4)
N3	−0.0861(8)	0.1829(8)	0.5744(6)	3.7(3)	N4′	0.040(1)	0.1121(9)	0.8738(7)	5.8(4)
N4	0.0695(9)	0.1213(8)	0.6674(6)	3.9(4)	C1′	0.217(2)	0.260(1)	0.9524(9)	6.7(7)
C1	0.244(1)	0.257(1)	0.7652(8)	4.1(5)	C2′	0.304(1)	0.328(2)	0.9930(8)	5.6(6)
C2	0.335(1)	0.322(1)	0.8022(7)	4.3(5)	C3′	0.280(2)	0.405(1)	0.9828(9)	6.5(6)
C3	0.321(1)	0.402(1)	0.7909(8)	4.8(5)	C4′	0.175(1)	0.388(1)	0.9392(8)	4.4(5)
C4	0.219(1)	0.393(1)	0.7486(7)	3.5(4)	C5′	0.118(1)	0.454(1)	0.9190(8)	4.3(5)
C5	0.165(1)	0.4628(9)	0.7290(7)	3.6(4)	C6′	0.020(1)	0.433(1)	0.8690(8)	4.4(5)
C6	0.065(1)	0.451(1)	0.9811(8)	4.3(5)	C7′	−0.047(1)	0.501(1)	0.8486(9)	4.8(5)
C7	0.004(1)	0.520(1)	0.6639(7)	4.3(5)	C8′	−0.127(1)	0.452(1)	0.7910(8)	4.4(5)
C8	−0.079(1)	0.479(1)	0.6115(8)	4.1(5)	C9′	−0.116(1)	0.360(1)	0.7823(8)	4.5(5)
C9	−0.077(1)	0.385(1)	0.5989(7)	3.9(5)	C10′	−0.188(1)	0.289(1)	0.7352(9)	5.3(6)
C10	−0.151(1)	0.320(1)	0.5482(9)	5.3(5)	C11′	−0.193(1)	0.201(2)	0.7537(9)	5.4(6)
C11	−0.156(1)	0.230(1)	0.5371(8)	4.5(5)	C12′	−0.280(2)	0.131(1)	0.694(1)	7.1(7)
C12	−0.234(1)	0.159(1)	0.4809(8)	5.0(5)	C13′	−0.267(2)	0.054(1)	0.712(1)	8.1(7)
C13	−0.210(1)	0.077(1)	0.4872(8)	4.0(4)	C14′	−0.167(2)	0.074(1)	0.767(1)	7.1(7)
C14	−0.117(1)	0.092(1)	0.5452(8)	4.6(5)	C15′	−0.117(2)	0.014(1)	0.804(1)	8.3(8)
C15	−0.072(1)	0.023(1)	0.5682(8)	5.4(6)	C16′	−0.020(2)	0.027(2)	0.852(1)	8.1(8)
C16	0.041(1)	0.039(1)	0.6292(9)	5.0(5)	C17′	0.028(2)	−0.041(2)	0.878(1)	9.7(9)
C17	0.060(1)	−0.035(1)	0.655(1)	6.2(6)	C18′	0.122(2)	0.002(2)	0.920(1)	11(1)
C18	0.146(1)	0.004(1)	0.7138(9)	6.2(6)	C19′	0.131(2)	0.099(1)	0.918(1)	6.6(6)
C19	0.149(1)	0.101(1)	0.7179(8)	5.4(5)	C20′	0.213(2)	0.167(2)	0.953(1)	8.9(6)
C20	0.229(1)	0.167(1)	0.7626(8)	4.5(5)	C25′	0.404(1)	0.298(1)	1.034(1)	8.8(7)
C25	0.432(1)	0.292(1)	0.8419(7)	5.1(5)	C26′	0.395(1)	0.291(1)	1.111(1)	10.3(8)
C26	0.499(1)	0.251(1)	0.794(1)	7.9(6)	C27′	0.359(1)	0.490(1)	1.0138(9)	6.1(5)
C27	0.407(1)	0.482(1)	0.8147(9)	6.0(5)	C28′	−0.037(1)	0.598(1)	0.8851(9)	7.5(6)
C28	0.020(1)	0.622(1)	0.6971(8)	6.3(5)	C29′	−0.214(1)	0.489(1)	0.7521(8)	5.5(5)
C29	−0.165(1)	0.521(1)	0.5719(9)	5.9(5)	C30′	−0.310(1)	0.488(1)	0.7886(9)	7.8(6)
C30	−0.140(1)	0.541(1)	0.5004(9)	8.5(7)	C31′	−0.369(1)	0.148(1)	0.635(1)	8.7(7)
C31	−0.324(1)	0.181(1)	0.4286(9)	7.7(6)	C32′	−0.336(2)	−0.038(1)	0.686(1)	11.4(9)
C32	−0.264(1)	−0.019(1)	0.4390(8)	5.8(5)	C33′	−0.408(3)	−0.048(2)	0.741(2)	22(2)
C33	−0.341(1)	−0.058(1)	0.476(1)	10.4(8)	C34′	−0.012(2)	−0.147(2)	0.858(2)	14(1)
C34	0.031(1)	−0.139(1)	0.620(1)	9.5(8)	C35′	−0.114(6)	−0.141(6)	0.901(7)	14(3)
C35	−0.064(2)	−0.168(1)	0.643(1)	12(1)	C35″	−0.047(5)	−0.151(5)	0.914(6)	12(3)
C36	0.222(1)	−0.039(1)	0.760(1)	8.7(7)	C36′	0.201(2)	−0.037(1)	0.964(1)	12(1)
CB1	0.216(1)	0.5580(9)	0.7620(8)	4.5(4)	CP1	0.486(2)	0.364(1)	0.365(2)	17[a]
CB2	0.260(1)	0.610(1)	0.7189(8)	5.7(5)	CP2	0.388(2)	0.316(1)	0.328(2)	22[a]
CB3	0.307(1)	0.698(1)	0.749(1)	6.9(6)	CP3	0.322(2)	0.284(1)	0.368(2)	21[a]
CB4	0.312(1)	0.745(1)	0.8230(9)	6.3(5)	CP4	0.355(2)	0.300(1)	0.445(2)	15[a]
CB5	0.270(1)	0.698(1)	0.8636(7)	5.2(5)	CP5	0.453(2)	0.348(1)	0.482(2)	20[a]
CB6	0.2251(1)	0.6033(9)	0.8344(8)	3.9(4)	CP6	0.518(2)	0.380(1)	0.441(2)	27[a]
CB1′	0.1654(9)	0.5495(8)	0.9488(7)	3.4(4)	CP7	0.498(4)	0.363(4)	0.563(3)	37[a]
CB2′	0.169(1)	0.598(1)	1.0222(9)	5.3(5)	CP8	0.428(2)	0.355(2)	0.596(2)	19[a]
CB3′	0.214(2)	0.683(2)	1.052(1)	8.5(7)					
CB4′	0.254(1)	0.736(1)	1.008(1)	6.3(5)					
CB5′	0.249(1)	0.694(1)	0.9360(9)	4.9(5)					
CB6′	0.2051(9)	0.602(1)	0.9077(7)	4.3(4)					

[a] Refined isotropically. Anisotropically refined atoms are given in the form of the isotropic equivalent displacement parameters defined as $(4/3)[a^2B(1,1) + b^2B(2,2) + c^2B(3,3) + ab(\cos\gamma)B(1,2) + ac(\cos\beta)B(1,3) + bc(\cos\alpha)B(2,3)]$.

thermore, these shifts are more important in the DPB than in the DPA series. Such a result can be interpreted as a greater π–π interaction between the two porphyrin chromophores,[31-34] due to the smaller rigid spacer. The same changes can be observed in monocopper and monozinc 1,8-bis(2,8,13,17-tetraethyl-3,7,12,18-tetramethylporphyrin-5-yl)biphenylene and 1,8-bis(2,8,13,17-tetraethyl-3,7,12,18-tetramethylporphyrin-5-yl)anthracene complexes for which the shifts are smaller than in the free base ($\Delta\lambda$[(DPB)H_4 – (MPP)H_2] = 20 nm, $\Delta\lambda$[(DPB)CuH_2 – (MPP)Cu] = 14 nm). The monocopper(II) compounds present typical "hypso" UV–vis spectra of regular copper(II) porphyrins.[35] The Q band shape for the (DP)CuH_2 complexes can be interpreted as the overlap of the bands due to the metalloporphyrin and those of the free base. The bands observed at 508 and 629 nm for (DPA)CuH_2 and 518 and 632 nm for (DPB)CuH_2 are attributed to $Q_y(1,0)$ and $Q_x(0,0)$ bands of the free base macrocycle. The two other middle absorptions observed in the region 530–580 nm correspond to the Q(1,0) and Q(0,0) bands of (Por)Cu and also to the $Q_x(1,0)$ and $Q_y(0,0)$ bands of the $(P)H_2$ core. The coordination of a second metal ion induces considerable spectral changes. The spectra exhibit characteristic absorption Soret bands, V and VI, of d-type hyperporphyrin,[35] and two supplementary absorptions, I and II, with a low intensity in the near infrared (Table 5).[36,37] Moreover, (DP)CuMnCl complexes show significant bathochromic shifts (5–10 nm) for the I–V bands, when compared to (Etio I)MnCl.[38] This shift results from the π–π interaction between the two macrocycles and eventually from any interactions between the two metal ions. The absorptions located at 534 and 406 nm are unambiguously attributable to the

(31) Collman, J. P.; Chong, A. O.; Jameson, G. B.; Oakley, R. T.; Rose, E.; Schmittou, E. R.; Ibers, J. A. *J. Am. Chem. Soc.* **1981**, *103*, 516–533.
(32) Chang, C. K.; Kuo, M.-S.; Wang, C.-B. *J. Heterocycl. Chem.* **1977**, *14*, 943–945.
(33) Chang, C. K. *J. Heterocycl. Chem.* **1977**, *14*, 1285–1288.
(34) Kagan, N. E.; Mauzerall, D.; Merrifield, R. B. *J. Am. Chem. Soc.* **1977**, *99*, 5484–5486.
(35) Gouterman, M. In *The Porphyrins*; Dolphin, D., Ed.; Academic: New York, 1978; Vol. III, pp 1–165.
(36) Gaughan, R.; Shriver, D. F.; Boucher, L. J. *Proc. Natl. Acad. Sci. U.S.A.* **1975**, *72*, 433–436.
(37) Boucher, L. J. *J. Am. Chem. Soc.* **1970**, *92*, 2725–2730.
(38) Edwards, L.; Dolphin, D. H.; Gouterman, M. *J. Mol. Spectrosc.* **1970**, *35*, 90–109.

Table 3. Selected Bond Distances (Å) and Angles (deg) for (DPB)CuMnCl·C_8H_{10}[a]

Mn–Cu	4.127(3)	Cu–N1′	2.00(1)
Mn–Cl	2.382(5)	Cu–N2′	1.97(1)
Mn–N1	2.034(9)	Cu–N3′	2.03(1)
Mn–N2	2.01(1)	Cu–N4′	1.99(1)
Mn–N3	2.027(9)		
Mn–N4	2.00(1)		
Cl–Mn–N1	94.5(3)	N1–Mn–N2	87.2(4)
Cl–Mn–N2	98.6(4)	N1–Mn–N4	90.9(4)
Cl–Mn–N3	97.8(3)	N2–Mn–N3	90.3(4)
Cl–Mn–N4	98.0(4)	N3–Mn–N4	88.1(5)
N1′–Cu–N2′	87.8(5)		
N1′–Cu–N4′	91.7(6)		
N2′–Cu–N3′	91.1(5)		
N3′–Cu–N4′	89.3(6)		

bond type[b]	mean[c]	angle type[b]	mean[c]
N–Ca	1.38(2)	Ca–N–Ca	105.3(2.2)
Ca–Cm	1.38(3)	N–Ca–Cb	110.2(2.5)
Ca–Cb	1.44(3)	N–Ca–Cm	124.2(2.2)
Cb–Cb	1.34(4)	Ca–Cb–Cb	107.1(2.1)
Cb–Cm1	1.51(2)	Cb–Cb–Cm1	122.8(2.3)
Cb–Cm2	1.59(4)	Cb–Cb–Cm2	128.4(1.8)
Cb–Ce1	1.53(4)	Ca–Cb–Cm1	125.8(4.7)
Ce1–Ce2	1.51(12)	Ca–Cb–Cm2	124.0(1.7)
		Cb–Cb–Ce1	124.4(3.0)
		Ca–Cb–Ce1	124.2(3.5)
		Cb–Ce1–Ce2	108.4(5.7)

[a] See Figure 1 for atom-labeling scheme. [b] Average of equivalent bonds and angles of the porphyrin rings. For steric reasons, the methyl groups close to the biphenylene connector are different from the others and are distinguished. The atoms are labeled as follows:

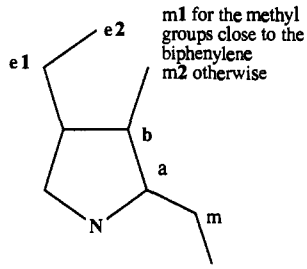

[c] The standard deviations of the mean values $\sigma(d)$ are the larger of the esd of a single observation and of $\sigma_{calc}(d) = [[N\sum d_i^2 - (\sum d_i)^2]/[N(N-1)]]^{1/2}$ for N equivalent bonds.

Scheme 1

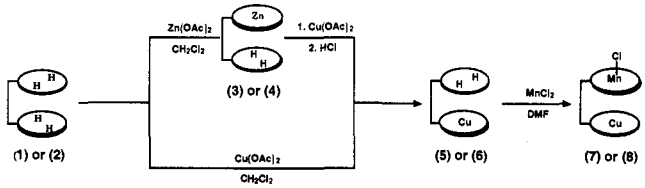

Q(1,0) and B(0,0) bands of the (*P*)Cu fragment. It is interesting to note that no significant shift is observed between the DPA and DPB series.

Electronic spectra of the low oxidation state (DP)$Cu^{II}Mn^{II}L$ complexes are similar to those of regular manganese(II) porphyrins[39] and show two Q bands in the region 535–571 nm as well as two Soret bands in the range of 398–443 nm (Table 5).

Infrared Spectroscopy. The monometallic complexes (DP)CuH_2 exhibit NH vibrations[40] at 3278 cm^{-1} for (DPA)CuH_2 and 3281 cm^{-1} for (DPB)CuH_2, whose intensity is half that of the free base. Heteronuclear (DP)CuMnCl complexes manifest typical vibrations due to the Mn–Cl bond in the region 270–274 cm^{-1}.[39,41]

(39) Boucher, L. J. *Coord. Chem. Rev.* **1972**, *7*, 289–329.
(40) Alben, J. O. In *The Porphyrins*; Dolphin, D., Ed.; Academic: New York, 1978; Vol. III, pp 323–345.
(41) Boucher, L. J. *J. Am. Chem. Soc.* **1968**, *90*, 6640–6645.

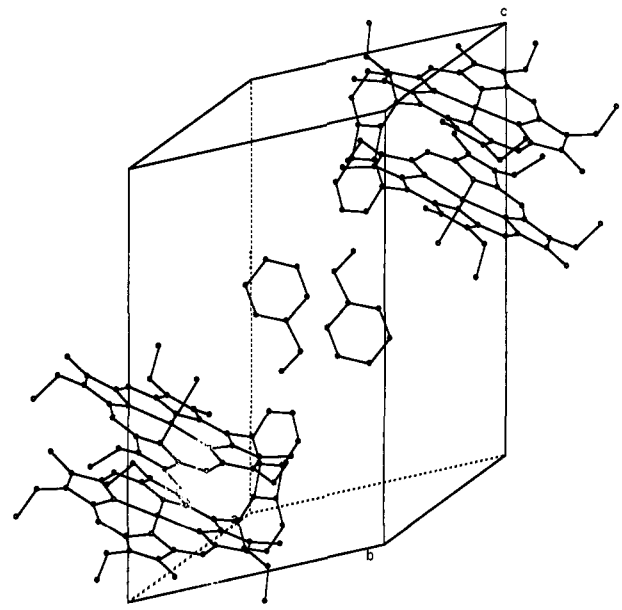

Figure 2. Unit cell view of (DPB)CuMnCl·C_8H_{10}.

Table 4. UV–Vis Data for the (DP)CuH_2 Complexes in CH_2Cl_2

	λ_{max} (nm) (10^{-3} ϵ (M^{-1} cm^{-1}))				
	Soret region	Q bands			
compound	B(0,0)	$Q_y(1,0)$	$Q_y(0,0)$	$Q_x(1,0)$	$Q_x(0,0)$
(DPA)CuH_2	391 (218.3)	508 (11.3)	534 (11.5)	570 (14.0)	629 (1.9)
(DPB)CuH_2	386 (212.9)	518 (10.2)	539 (9.6)	575 (10.4)	632 (1.6)

No vibration corresponding to the Mn–N (imidazole) bond is observed for the (DP)CuMnL derivatives.

Mass Spectrometry. Mass spectral data are given in the Experimental Section. The molecular peak is observed for the monometallic (DP)MH_2 and bimetallic (DP)CuMnCl complexes. However, fragmentation reactions are critically dependent on the coordination scheme of the central metal. Thus, for (DP)CuH_2 and (DP)CuZn, the molecular peak is the base peak, whereas for (DP)CuMnCl the base peak corresponds to $[M - Cl]^+$ and the relative intensity of the molecular peak ranges from 15% to 30%. Such a fragmentation is usually observed for five-coordinated metalloporphyrins. No molecular peak is detected for the low oxidation state complexes (DP)$Cu^{II}Mn^{II}L$ due to the extreme lability of the manganese axial ligand. The base peak corresponds to the $[(DP)CuMn]^+$ fragment.

Magnetic Study. Figure 4 illustrates the temperature dependence of the magnetic moment of the two (DP)CuMnCl compounds. For (DPA)CuMnCl the moment amounts to 5.06 μ_B at room temperature and slightly increases to 5.3 μ_B when the temperature decreases to around 100 K. At lower temperatures the moment increases more strongly to reach a maximum value of 5.98 μ_B at 4 K. A steep decrease is observed at even lower temperatures. Analysis of the curves of the magnetic susceptibility vs the inverse of the temperatures reveals two linear domains: at temperatures higher than 40 K with a Curie constant of 3.42 and in the range 4–18 K with a Curie constant of 4.72. Both the value of the magnetic moment and the Curie constant in the high-temperature range are consistent with magnetically independent spins of the manganese ($S = 2$) and the copper ($S = 1/2$) atoms. Moreover, the maximum value reached at 4 K as well as the Curie constant correspond to a system with a 5/2 spin state. Accordingly, the behavior of (DPA)CuMnCl appears dominated by a moderate ferromagnetic interaction which leads to a 5/2 ground state.

In the high-temperature range (from 30 to 100 K), (DPB)-CuMnCl has a magnetic moment of around 5.1 μ_B (Figure 4); at temperatures lower than 50 K this moment slightly increases

Table 5. UV–Vis Data for the Heterobimetallic Complexes in CH_2Cl_2

	λ_{max} (nm) ($10^{-3}\epsilon$ (M^{-1} cm^{-1}))							
	Soret region			Q bands				
compound	VI	B(0,0)	V	Q(1,0)	Q(0,0)	IV	II	I
(DPA)CuZn		390 (337.4)		536 (22.1)	572 (23.7)			
(DPB)CuZn		387 (321.3)		539 (15.6)	572 (15.5)			
(DPA)CuMnCl	361 (116.7)	406 (136.1)	479 (34.6)	534 (11.4)	568 (17.0)		691 (0.6)	789 (0.9)
(DPB)CuMnCl	362 (124.5)	404 (90.7)	482 (25.9)	533 (10.5)	569 (13.7)		692 (0.6)	789 (0.9)
(DPA)CuMn(L)[a]		405 (299.4)	437 (71.9)	535 (16.0)	566 (26.8)			
(DPB)CuMn(L)[a]		398 (234.9)	443 (35.2)	541 (12.9)	571 (20.2)			

[a] In degassed toluene under argon.

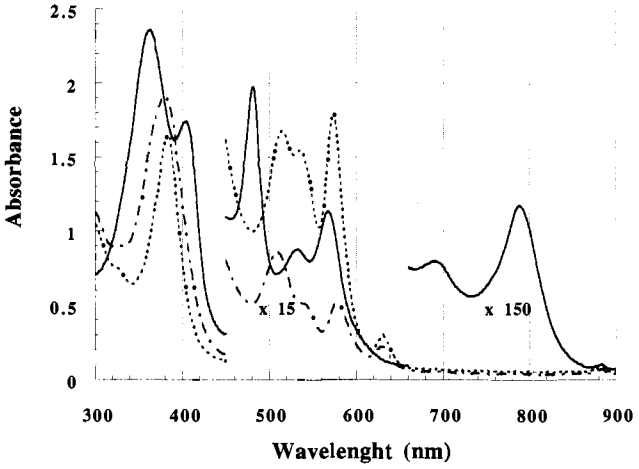

Figure 3. UV–vis spectra of $(DPB)H_4$ (– – –), $(DPB)CuH_2$ (- - -), and (DPB)CuMnCl (—) recorded in CH_2Cl_2.

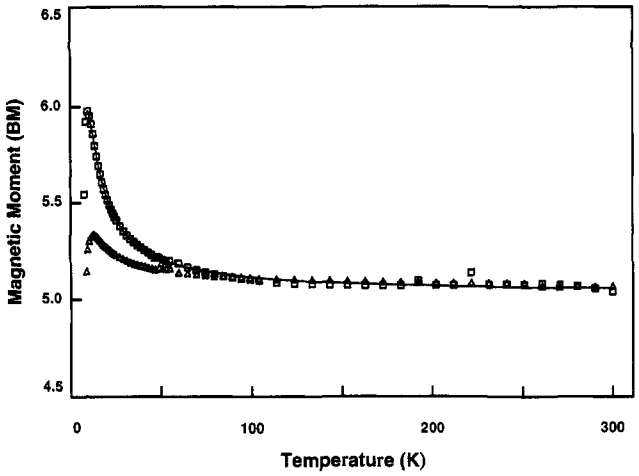

Figure 4. Effective magnetic moment vs temperature (T) for (DPA)CuMnCl (□) and (DPB)CuMnCl (△) (the solid line represents the best least-squares fit of the data).

to reach a maximum of 5.34 μ_B at 7 K. The curve of the magnetic susceptibility vs the inverse of the temperature is linear over the whole domain with a Curie constant of 3.42. Such a behavior is consistent with the two metal spins being essentially independent; i.e., if there is any exchange interaction between the two ions, it must be notably weaker than in (DPA)CuMnCl.

Magnetic susceptibility studies of manganese(III) tetraphenylporphinato complexes[42] have shown that their behavior is dominated at low temperature by an axial zero-field splitting (ZFS) (D) of around 2–3 cm^{-1}. In the case of (DPA)CuMnCl, since the magnetic exchange interaction (J) appears so strong that the 5/2 ground state is fully populated at low temperatures, we have assumed that it was higher than the ZFS. The resulting ground ($S = 5/2$) and excited ($S = 3/2$) states were then submitted

(42) Behere, D. V.; Mitra, S. *Inorg. Chem.* **1980**, *19*, 992–995.

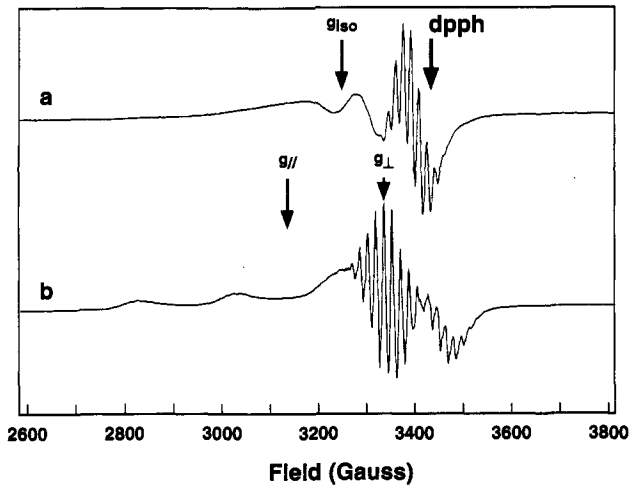

Figure 5. ESR spectra of $(DPB)(CuH_2$ at (a) 298 K and (b) 100 K in toluene.

to the effect of axial ZFS D_g and D_e, respectively. The corresponding theoretical magnetic susceptibility deduced from Van Vleck's equation was then used to fit the experimental data. Very good agreement was obtained (solid line in Figure 4) with the following set of parameters: $J = 4.7$ cm^{-1}, $D_g = 1.6$ cm^{-1}, and $D_e = 2.9$ cm^{-1}. The values of the ZFS of the two states (D_g and D_e) are compatible with the one of an isolated Mn^{III} ion in a porphyrin, and they are actually lower than the exchange interaction.

We could expect that the exchange interaction is lower in (DPB)CuMnCl, and similar analysis was attempted under the assumption that J is lower than D, the Mn^{III} axial ZFS parameter. Simulation of the data did not provide any valuable result. The reason for the failure of this analysis is probably to be found in the respective values of J and D; actually, if both parameters are of the same order of magnitude, such a simple analysis is not valid anymore and the solution of the problem requires simulation of the magnetization data using full diagonalization of the corresponding matrices. This work is in progress.

ESR Spectroscopy. The isotropic and anisotropic ESR spectra of $(DP)CuH_2$ and (DP)CuMnCl (Figures 5 and 6) are typical of Cu^{II} complexes in a ^2D ground state within a tetragonal field. The isotropic spectrum of $(DPB)CuH_2$ presents a hyperfine coupling (Figure 5a) due to the interaction between the unpaired electron and the copper nuclear spin ($I_{Cu} = 3/2$). Moreover, the nuclear spin of nitrogen ($I_N = 1$) generates a superhyperfine coupling of nine lines located at high field.[43] In frozen solution, the anisotropic spectrum shows the superhyperfine perpendicular signals and the overlap of parallel and perpendicular lines (Figure 5b).[43–45] The $g_\parallel$, $A_\parallel^{Cu}$, $A_\perp^{N}$, and $A_\parallel^{N}$ parameters have been

(43) Yokoi, H.; Iwaizumi, M. *Bull. Chem. Soc. Jpn.* **1980**, *53*, 1489–1492.
(44) Neiman, R.; Kivelson, D. *J. Chem. Phys.* **1961**, *35*, 156–161.
(45) Findlay, M. C.; Dickinson, L. C.; Chien, J. C. W. *J. Am. Chem. Soc.* **1977**, *99*, 5168–5173.

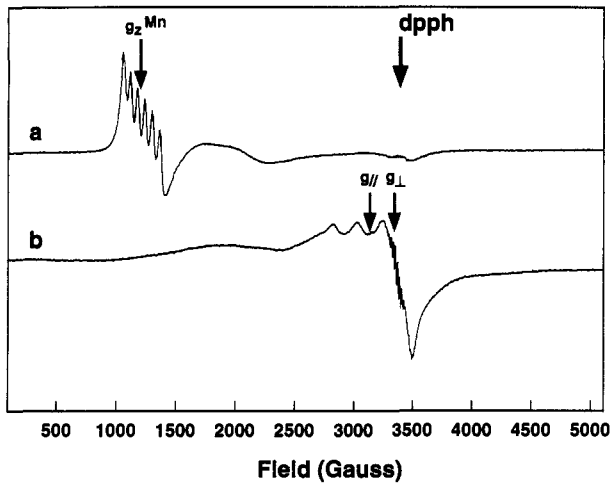

Figure 6. ESR spectra of (a) (DPB)CuMnCl and (b) (DPA)CuMnCl at 100 K in toluene.

determined (Table 6). These data are in good agreement with those previously reported for copper monoporphyrins.[46]

The coordination of the second porphyrin moiety induced significant spectral changes, and it is noteworthy that no spectrum is observed at room temperature for the (DP)CuMnCl complexes. At this temperature, the two ions are magnetically independent and relaxation effects are the probable cause of the disappearance of the ESR spectra. The ESR spectrum of (DPA)CuMnCl is totally distorted at 100 K compared to the copper(II) monoporphyrins and monocopper Pacman derivatives (Figure 6a). Such a change has already been reported for the copper(II) *α,β-meso*-dinitrooctaethylporphinato complex[47] for which a dimeric structure has been proved. According to the structure of cofacial porphyrins in the DPA series, this pattern can result from a significant interaction between copper and manganese ions, and to a lesser extent to a π–π macrocycle interaction. The shape of the spectrum is unaltered when the temperature is decreased to very low temperatures. Figure 7 illustrates the ESR spectrum of (DPA)CuMnCl in toluene at temperatures lower than 30 K. The 26 K spectrum exhibits features associated with a copper(II) ion. When the temperature is lowered, this signal grows and simultaneously three additional features appear at $\mathbf{g} \approx 1.5$, 1.84, and 2.6, respectively. The latter feature can be detected only at the lowest temperatures and as a broad shoulder on the main $\mathbf{g} \approx 2.07$ line. Owing to the difficulty in observing this signal, the occurrence of other features at lower field cannot be excluded. Anyhow, the ESR experiment demonstrates the presence of a new (ESR active) state with several transitions over a large field domain. Moreover, the disappearance of the spectrum of this state at still low temperature (T = 30 K) is consistent with the presence of an excited state very close in energy. This behavior is quite in line with the results of the susceptibility study.

The spectrum of (DPB)CuMnCl is not observable at room temperature but appears at around 100 K (Figure 6a) and persists down to liquid helium temperatures. It comprises two components: a six-line feature at $\mathbf{g} \approx 5.68$ and a multiline pattern at $\mathbf{g} \approx 2$. The latter should be due to the copper(II) porphyrin core. The splitting of the high-field component takes its origin in the hyperfine coupling with the manganese nuclear spin (I_{Mn} = 5/2, a = 59 G).

A careful study of the temperature dependence of the spectrum has shown that the two components behave differently at temperatures lower than 10 K: while the intensity of the $\mathbf{g} \approx 2$ feature follows the Curie law down to the lowest available temperature (around 4 K), the other one departs from the linear intensity vs T^{-1} behavior at T = 10 K. The linear dependence of the intensity of both components vs the square root of the power down to 4 K warrants that no saturation effect is disturbing the experiment. Firstly, the occurrence of a six-line perpendicular component near $g_\perp \approx 6$ would suggest the presence of a manganese(II) species. However, we believe that this interpretation is not valid because (i) the characteristic component exhibiting manganese hyperfine splitting in the parallel region[48] at $\mathbf{g} \approx 2$ is lacking and (ii) the hyperfine splitting of the perpendicular feature $A_\perp = 55 \times 10^{-4}$ cm^{-1} is too low since, for manganese(II) porphyrins, the usual value is close to $A_\perp = 73 \times 10^{-4}$ cm^{-1}. Secondly, EPR spectra of high-spin (S = 2) manganese(III) species have been detected only in special instances such as, for example, when Mn^{3+} substitutes Ti^{4+} in titanium oxides (rutile[49] or $SrTiO_3$[50]). So far manganese(III) porphyrins have not shown any EPR spectrum,[42] and it is not likely that the present spectrum is associated with a pure manganese(III) species. Thirdly, the high $g_\perp$ value observed here is inconsistent with a manganese(IV) porphyrin. Actually for such compounds possessing a high-spin d^3 electronic configuration which exhibit axial EPR spectra the $g_\perp$ values are near 4.[51] Moreover, the possibility that the present spectrum is associated with a 3/2 state resulting from an antiferromagnetic coupling between the two ions is definitely ruled out by the magnetic susceptibility study which points to a ferromagnetic interaction and conversely excludes the occurrence of such a state populated in so wide a range of temperature. However, this study is consistent with a weak ferromagnetic interaction of the order of magnitude of the ZFS of the manganese(III) ion, ca.1 cm^{-1}. It is thus possible that this interaction is sufficient to mix the copper $|\pm 1/2\rangle$ spin states and the manganese $|\pm 2\rangle$ spin states (resulting from the ZFS[42]), leading to the following four spin states: $|\pm 2 \pm 1/2\rangle$. The EPR spectrum would correspond to transitions between these states. The low value of the perpendicular hyperfine interaction, $A_\perp = 55 \times 10^{-4}$ cm^{-1}, supports this interpretation. Actually, this value corresponds exactly to the one expected from the ratio of the projections of the manganese (S = 2) spin and that of the ground state (S = 5/2) in the case of a strong exchange.[52] Although this case does not correspond to the present situation, it is possible that a similar relationship holds. Multifield magnetization studies are planned to determine the values of the exchange interaction J and the ZFS parameter D in order to find which of the weak and intermediate coupling situations operates in the present case, so that the EPR spectra can be simulated.

ESR spectra of (DP)$Cu^{II}Mn^{II}$L complexes obtained at 100 K are shown in Figure 8. The spectral shape of (DPB)$Cu^{II}Mn^{II}$L is typical of manganese(II) porphyrin.[21,48,53] The X band spectrum exhibits two signals at $g_\perp \approx 6$ and $g_\parallel \approx 2$ with hyperfine coupling (I_{Mn} = 5/2) $A_\perp$ = 70 G and $A_\parallel$ = 117 G (Table 7). The presence of small side bands may indicate a weak rhombic distortion. The values of g can be compared to those observed for a d^5 (S = 5/2) high-spin system with a zero-field splitting parameter (D) higher than the frequency of the X band ($\nu > 0.31$ cm^{-1}). For example, Q band measurements for (TPP)Mn(Py)[54] and Mn^{II}Hb[48] give $D^{Mn} = 0.55$ cm^{-1} and $\lambda \approx 0.01$. The parallel lines of the Mn^{II} in (DPA)$Cu^{II}Mn^{II}$L are masked by the signal of copper(II), whose

(46) Guzy, C. M.; Raynor, J. B.; Symons, M. C. R. *J. Chem. Soc. A* **1969**, 2299–2303.
(47) Chikira, M.; Kon, H.; Hawley, R. A.; Smith, K. M. *J. Chem. Soc., Dalton Trans.* **1979**, 245–249.
(48) Yonetani, T.; Drott, H. R.; Leigh, J. S., Jr.; Reed, G. H.; Whaterman, M. R.; Asakura, T. *J. Biol. Chem.* **1970**, *245*, 2998–3003.
(49) Gerritsen, H. J.; Sabisky, E. S. *Phys. Rev.* **1963**, *132*, 1507–1512.
(50) Serway, R. A.; Berlinger, W.; Müller, K. A.; Collins, R. W. *Phys. Rev. B* **1977**, *16*, 4761–4768.
(51) Camenzind, M. J.; Hollander, F. J.; Hill, C. L. *Inorg. Chem.* **1983**, *22*, 3776–3784.
(52) (a) $A^{5/2}_{Mn} = a_{Mn}(2/2.5) = 55 \times 10^{-4}$ cm^{-1} if $a_{Mn} = 73 \times 10^{-4}$ cm^{-1}; the contribution of the copper ion to the hyperfine splitting would be $A^{5/2}_{Cu} = a_{Cu}(0.5/2.5) = 6 \times 10^{-4}$ cm^{-1} if $a_{Cu} = 32 \times 10^{-4}$ cm^{-1}. Accordingly it might be too small to be resolved. (b) Bencini, A.; Gatteschi, D. *EPR of Exchange Coupled Systems*; Springer Verlag: Berlin, 1990.
(53) Yonetani, T.; Yamamoto, H.; Erman, J. E.; Leigh, J. S., Jr.; Reed, G. H. *J. Biol. Chem.* **1972**, *247*, 2447–2455.
(54) Hoffman, B. M.; Weschler, C. J.; Basolo, F. *J. Am. Chem. Soc.* **1976**, *98*, 5473–5482.

Table 6. ESR Data for Different Copper Complexes in Toluene at Room Temperature and 100 K

compound	g_{iso}	$g_{\parallel}$	$g_{\perp}$	A_{iso}^{Cu} (10^4 cm^{-1})	A_{iso}^{14N} (10^4 cm^{-1})	$A_{\parallel}^{Cu}$ (10^4 cm^{-1})	$A_{\perp}^{14N}$ (10^4 cm^{-1})	$A_{\perp}^{Cu}$ (10^4 cm^{-1})	$A_{\parallel}^{14N}$ (10^4 cm^{-1})
(MPP)Cu	2.110	2.194	2.068	87.3	14.9	183.2		39.3	
(OEP)Cu[a]	2.097	2.186	2.053	86.6		207.0		26.4	
(DPA)CuH$_2$	2.112	2.185	2.075	84.6	14.9	188.8		32.5	
(DPB)CuH$_2$	2.114	2.186	2.078	84.6	14.8	190.7	13.0	31.5	18.4
(DPA)ZnCu	2.114	2.195	2.073	85.0	14.8	184.1	13.0	35.5	18.4
(DPB)ZnCu	2.114	2.193	2.074	86.3	14.8	185.4	13.2	36.7	18.2
(DPA)CuMnCl		2.201	2.075			188.8		32.5	

[a] From Chikira, M.; Kon, H.; Hawley, R. A.; Smith, K. M. *J. Chem. Soc., Dalton Trans.* **1979**, 245–249.

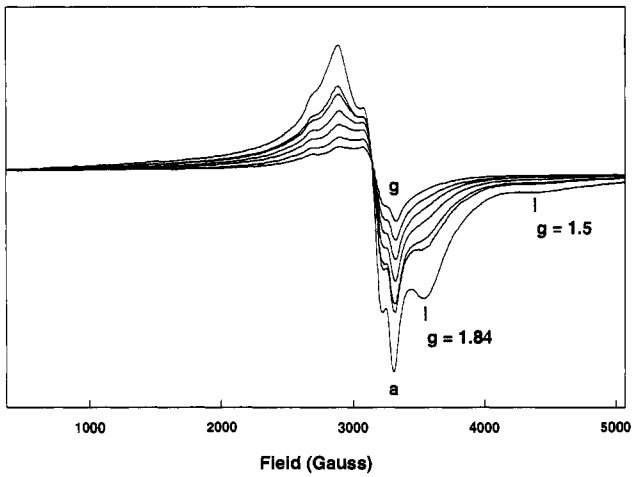

Figure 7. ESR spectra of (DPA)CuMnCl in toluene at different temperatures: (a) 3.8 K, (b) 4.4 K, (c) 5.2 K, (d) 7.4 K, (e) 10.5 K, (f) 17.2 K, (g) 26 K.

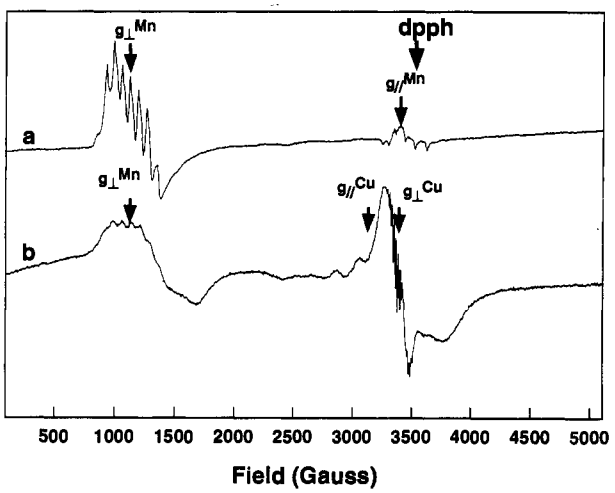

Figure 8. ESR spectra of (a) (DPB)Cu^{II}Mn^{II}L and (b) (DPA)Cu^{II}Mn^{II}L at 100 K in toluene.

spectral pattern is similar to that observed for the (DPA)Cu^{II}-Mn^{III}Cl precursor.

It is remarkable that no copper(II) signal appears for (DPB)Cu^{II}Mn^{II}L. This difference should be attributed to a different value of the relaxation time for the copper electronic transitions due to the proximity of the second metal ion. However, the same observation is done for the oxygenated compound (DPB)CuMn(O$_2$) (vide infra) and the (DPB)CuMnCl precursor for which a cooperative effect has been proved by means of magnetic and ESR studies. The absence of a copper(II) signal should also be attributed to a weak cooperative effect occurring for (DPB)Cu^{II}Mn^{II}L. However, we have to point out that these interactions observed for the copper(II)–manganese(II) systems are weak at room temperature and 100 K since an intense coupling only appears at 4 K. Thus, the two series Cu(II)–Mn(II) and Cu(II)–Mn(III) show a similar magnetic behavior.

Reactivity of (DP)Cu^{II}Mn^{II}L toward Dioxygen. In the metalloporphyrin series only a few examples of reversible binding of dioxygen have been observed because instantaneous oxidation and dimerization occur for most of the systems. The reactivity of both (DP)Cu^{II}Mn^{II}L compounds toward dioxygen has been studied by ESR spectroscopy at 100 K in toluene and in the presence of an excess of the bulky ligand L. This study was performed by generating (DP)Cu^{II}Mn^{II}L in situ to prevent any formation of a Mn^{III} complex, and an experiment consists in bubbling dioxygen at room temperature for 1 min through the solution and then bubbling argon for 5 min.

In the presence of an excess of ligand L and dioxygen, (DPA)Cu^{II}Mn^{II}L is irreversibly oxidized to a Mn^{III} complex. Indeed the ESR spectrum indicates the disappearance of the Mn^{II} signal, but no new absorption is observed. The UV–vis spectrum shows a band at 480 nm typical of manganese(III) porphyrins. From these studies, it appears that (DPA)Cu^{II}Mn^{II}L does not show a reversible reaction with dioxygen at room temperature. So the DPA complex tends to behave like monoporphyrinic compounds for which a reversible reaction is shown only at low temperature (−78 °C). In contrast under the same experimental conditions after exposure to dioxygen, the ESR spectrum of (DPB)Cu^{II}Mn^{II}L disappears and new lines at $\mathbf{g}_1 \approx 5.44$, $\mathbf{g}_2 \approx 2$, and $\mathbf{g}_3 \approx 1.45$ are observed (Figures 9 and 10).[54]

Deoxygenation of the resulting solution partially restores the original spectrum (Figure 9c); the formation of a degradation product weakly enhances the signal close to $\mathbf{g} = 2$. The low-field region of the spectrum for the oxygenated species (Figure 10) corresponds to the overlap of two sextets ($g_y^{eff} = 5.432$, $A_y = 57.4$ G and $g_z^{eff} = 5.445$, $A_z = 88.8$ G). In fact, we observe the superposition of two Kramers doublets with different $\mathbf{g}$ and $\mathbf{A}$ values. Such a spectrum has already been observed with TPP and OEP ligands, and it is well established that this spectrum feature occurs for an oxygenated manganese complex.[54] However, the oxygenation of manganese(II) monoporphyrin complexes has been studied at −78 °C because of the high instability of the oxygenated compounds at room temperature, while the reactivity of the DPB complex toward dioxygen has been studied at room temperature. In contrast to the manganese monoporphyrin derivatives, the copper porphyrin tends to stabilize the dioxygen adduct through a cooperative effect between the two metals.

It is well known that the coordination of dioxygen for five-coordinated manganese porphyrins proceeds via a ligand exchange process (Scheme 2). Such a competition between dioxygen and the ligand is thought to be due to the large anionic radius of Mn^{II} that induces the displacement of the manganese ion from the mean porphyrin plane.[55] According to this exchange process, coordination of dioxygen occurs outside of the cavity (Scheme 2). Moreover, if we suppose that coordination of dioxygen occurs inside the cavity, any intermolecular dimerization process giving a μ-oxo species, (Por)Mn–O–Mn(Por), should be excluded and stabilization of dioxygen should have been observed also for the (DPA)CuMn(O$_2$) complex, which is untrue. So it seems that the metal–metal distance and therefore the cooperative effect

(55) Kirner, J. F.; Reed, C. A.; Scheidt, W. R. *J. Am. Chem. Soc.* **1977**, *99*, 2557–2563.

Table 7. ESR Data for the Copper–Manganese Complexes in Toluene at 100 K

compound	$g_{\parallel}^{Cu}$	$g_{\perp}^{Cu}$	$A_{\parallel}^{Cu}$ (10^4 cm^{-1})	$A_{\perp}^{Cu}$ (10^4 cm^{-1})	$g_{\parallel}^{Mn}$	$g_{\perp}^{Mn}$	$A_{\parallel}^{Mn}$ (10^4 cm^{-1})	$A_{\perp}^{Mn}$ (10^4 cm^{-1})
(DPA)CuMnCl	2.201	2.075	188.8			5.684		55.1
(DPB)CuMnCl	≈ 2					6.046		70.1
(DPA)CuMn(L)	2.180	2.075	184.4	32.5	2.018	6.050	110	63.5
(DPB)CuMn(L)								

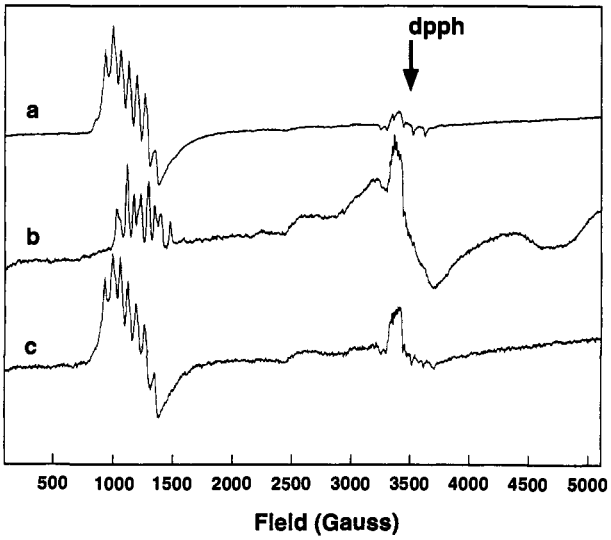

Figure 9. ESR spectra at 100 K of (DPB)Cu^{II}Mn^{III}L (a) in degassed toluene, (b) after dioxygen bubbling for 1 min, and (c) after argon bubbling for 5 min.

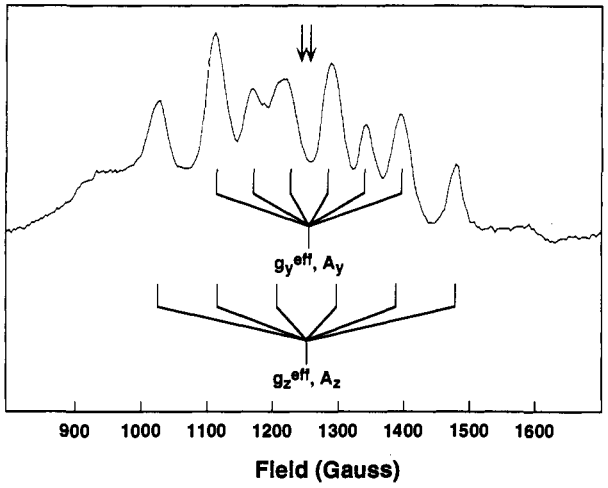

Figure 10. Low-field region of ESR spectrum of (DPB)CuMn(O_2) in dioxygen-saturated toluene solution at 100 K.

Scheme 2

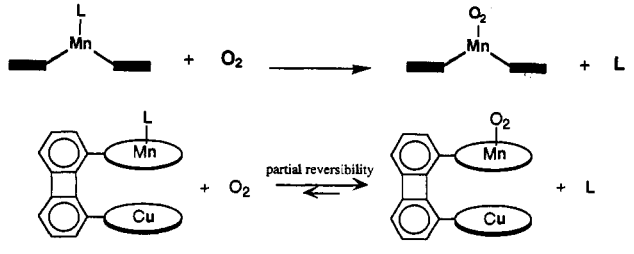

between the two central metals are the major factors responsible for the stabilization of (DPB)CuMn(O_2).

The spectrum for the oxygenated complex (Figures 9b and 10) does not correspond to a superoxidic adduct as observed in the cobalt(II) porphyrin series. The spectrum is more similar to those observed for complexes possessing a d^3 configuration (S = 3/2). Thus, the oxygenated adduct can be viewed as a high-spin system (S = 3/2) with a large zero-field splitting ($D > h\nu \approx 0.31$ cm^{-1}) and a prominent rhombic distortion (E). Such a system could be formulated as (DPB)CuMn^{IV}(O_2) where the manganese atom in a IV oxidation state is bonded to a peroxide moiety.

McGarvey resolved the Hamiltonian for S = 3/2 systems to calculate the **g** and λ parameters (as already defined, λ = E/D), and the **g** tensor (**g** = 1.99) and λ parameter (λ = 0.33) were determined according to McGarvey's solutions. The λ value corresponds to a quasi perfect rhombicity for the oxygenated species (DPB)CuMn(O_2). The D parameter has also been calculated according to the following equation:[54] $\Delta = 2D(1 + 3\lambda^2)^{1/2}$, Δ being the energy separation between the two Kramers doublets of the four spin states in the absence of a magnetic field (Δ = 5.82 cm^{-1} for (TPP)Mn(O_2);[54] see Table 8). As expected this value is largely superior to the microwave frequency. These data agree well with a peroxide arrangement as already described for (OEP)Ti(O_2)[56] and [K(K222)][(TPP)Mn(O_2)][57] complexes (Chart 1).

All these results show without any ambiguity the formation of an oxygenated complex, (DPB)CuMn(O_2), at room temperature. We can therefore suggest that such a coordination of dioxygen occurs through the mean of metal–metal interactions which stabilize the four valency of manganese in the dioxygen adduct.

Concluding Remarks. The Pacman porphyrin series appear to be good model molecules to observe π–π interactions between the two porphyrin units as well as metal–metal interactions. The susceptibility data show that the exchange interaction is ferromagnetic (the decrease of the magnetic moment values at very low temperatures is most probably due to intermolecular interactions) and that it is far greater in (DPA)CuMnCl than in (DPB)CuMnCl despite the fact that the Mn–Cu distance is shorter in the latter.[58] It is noteworthy that in the biscopper derivatives the magnetic exchange interaction was estimated to ca. 0.5 cm^{-1} for both ligands.[58] The interaction is supposed to be mostly dipolar. Owing to the weak coupling, a comparable situation is quite plausible in (DPB)CuMnCl. In the case of (DPA)CuMnCl the interaction is both stronger and ferromagnetic. The sign of this interaction can be explained by considering the magnetic orbitals involved. In the present structural arrangements, the respective electronic configurations of the two ions are $(d_{xy})^1(d_{yz})^1(d_{xz})^1(d_{z^2})^1$ for the high-spin Mn^{III} ion and $(d_{x^2-y^2})^1$ for the Cu^{II} ion. By assuming a symmetry plane perpendicular to the porphyrin planes and running through the anthracenyl group (local C_s symmetry), it can be seen that a single interaction is allowed between the copper $d_{x^2-y^2}$ orbital and the manganese $d_{yz} - d_{xz}$ combination mediated by the π orbitals of the anthracenyl residue. A weak overlap is associated with this interaction. On the other hand, the three other magnetic orbitals based on manganese d_{xy}, d_{z^2}, and $d_{yz} + d_{xz}$ orbitals must give rise to ferromagnetic contributions involving significant overlap densities. It is therefore reasonable that the latter interactions outweigh the former one, leading to an overall ferromagnetic coupling between the two ions.

It is demonstrated that (DPB)CuMnL is a better candidate for reversible coordination of dioxygen compared to manganese(II) monoporphyrins. These results also suggest that the copper–

(56) Guilard, R.; Latour, J.-M.; Lecomte, C.; Marchon, J.-C.; Protas, J.; Ripoll, D. *Inorg. Chem.* **1978**, *17*, 1228–1237.
(57) VanAtta, R. B.; Strouse, C. E.; Hanson, L. K.; Valentine, J. S. *J. Am. Chem. Soc.* **1987**, *109*, 1425–1434.
(58) Eaton, S. S.; Eaton, G. R.; Chang, C. K. *J. Am. Chem. Soc.* **1985**, *107*, 3177–3184.

Table 8. Spin-Hamiltonian Parameters[a] for Some $S = 3/2$ Complexes

compound	$\|D\|$ (cm^{-1})	λ	g^{Mn}	$\|A\|$ (10^4 cm^{-1})	$\|B\|$ (10^4 cm^{-1})
(DPB)$CuMnO_2$	2.52	0.331	1.990 ± 0.003	53.6 (*y*)	83 (*z*)
(TPP)MnO_2[b]	2.48	0.325	1.995 ± 0.005	53.1 (*y*)	82 (*z*)
trans-$Cr(en)_2A_2^{n+}$[c]	0.41–0.50	0.023–0.216	1.97–1.99		

[a] Symbols are defined as reported in footnote *b*. [b] Taken from Hoffman, B. M.; Weschler, C. J.; Basolo, F. *J. Am. Chem. Soc.* **1976**, *98*, 5473–5482. [c] *trans*-$Cr(en)_2A_2^{n+}$ = *trans*-dichloro-, -diaquo-, -dihydroxo-, and -dithiocyanatobis(ethylenediamine)chromium(III) chloride, taken from Hempel, J. C.; Morgan, L. O.; Burton Lewis, W. *Inorg. Chem.* **1970**, *9*, 2064–2072.

Chart 1

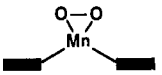

manganese cooperativity stabilizes the peroxide manganese moiety and is able to model synthetic oxygen carriers.

Acknowledgment. The support of the CNRS is gratefully acknowledged. We thank Professor James P. Collman and Dr. Jean-Jacques Girerd for helpfuldiscussions. C.L. and N.B. are grateful to D. Bayeul for technical help.

Supplementary Material Available: Tables of anisotropic thermal motion parameters, full bond distances and angles, positional parameters for hydrogen atoms, and least-squares planes for (DPB)$CuMnCl \cdot C_8H_{10}$ (11 pages); a table of observed and calculated structure factors for (DPB)$CuMnCl \cdot C_8H_{10}$ (25 pages). This material is contained in many libraries on microfiche, immediately follows this article in the microfilm version of the journal, and can be ordered from the ACS; see any current masthead page for ordering information.